Heavy singlet fermionic dark matter with Z_4 symmetry

XinXin Qi[1,*] and Hao Sun[1,†]

[1] *Institute of Theoretical Physics, School of Physics, Dalian University of Technology, No.2 Linggong Road, Dalian, Liaoning, 116024, P.R.China*

We revisited the singlet fermionic dark matter model in this work, where a Majorana fermion χ carrying Z_4 charge is assumed as the DM candidate. A new singlet scalar S_0 with a non-zero vacuum expectation value is also introduced to the SM so that χ can obtain mass after spontaneous symmetry breaking. We focus on the secluded DM region for the model, where interactions between DM and SM particles can be negligible. We have a new Higgs h_2 in the model, and the mixing angle of h_2 with the SM Higgs will play an important role in determining DM production, depending on the mass hierarchy between the new Higgs mass and the DM mass. We study DM relic density as a function of the model's four free parameters and estimate the viable parameter space under DM relic density constraint as well as direct detection constraint. We focus on the heavy DM mass region, and our analysis indicates that the mixing angle does not necessarily need to be very small in the secluded dark matter scenario, which offers potential for probing such models in future collider experiments.

arXiv:2606.11936v2 [hep-ph] 15 Jun 2026

I. INTRODUCTION

The nature of dark matter (DM) remains one of the most profound mysteries in modern physics. From a particle physics perspective, DM is assumed to consist of non-baryonic, cold particles not included in the Standard Model (SM). Among the most widely studied candidates is the weakly interacting massive particle (WIMP), which can naturally achieve the correct DM relic abundance via the thermal freeze-out mechanism. However, current direct detection experiments have found no evidence for WIMPs [1, 2], and these null results impose stringent constraints on the interaction cross section between DM and SM particles. In particular, WIMP models typically require a large annihilation cross section to reproduce the observed DM relic density, while direct detection experiments force the corresponding couplings to be small.

One possible solution to alleviate the tension is secluded DM [3], where the dominant annihilation of DM occurs into a hidden sector mediator rather than directly into SM particles in this scenario. According to [3], the secluded DM does not directly participate in the interactions of the SM, but instead belongs to a dark sector, which couples weakly to the SM through a portal. The annihilation of DM primarily takes place in the dark sector, and these dark sector particles will subsequently decay into SM particles via the portal coupling. The coupling between dark matter and the SM particles can be extremely weak, thereby naturally suppressing the direct detection cross section and explaining why experiments with extremely low backgrounds have so far failed to observe the DM signal. Meanwhile, the coupling of the dark sector particles can be sufficiently strong to ensure the correct DM relic density through annihilation in the early universe, and even provide rich indirect detection signals through mechanisms such as Sommerfeld enhancement and resonances [4–6].

Discussions of secluded dark matter (DM) can be found in refs. [5, 7–19]and so on. In this work, we consider a fermionic DM candidate in the secluded regime, assuming a Majorana fermion χ with a Z_4 charge. The Z_4 symmetry forbids a bare Majorana mass for χ but allows a Yukawa interaction with a new singlet scalar S_0, whose vacuum expectation value generates the DM mass upon spontaneous symmetry breaking.

The singlet fermionic DM model has been extensively studied for its simplicity [20–35] and so on, and its secluded scenario [36, 37] significantly weakens the correlation between thermal freeze-out and direct detection rates. In our setup, DM annihilation is dominated by $\chi\chi \to h_2 h_2$ via the new scalar mediator h_2, while the coupling to Standard Model (SM) particles is governed by the scalar mixing angle θ. This structure allows the correct relic abundance to be obtained even when the direct detection cross section is suppressed by a small mixing angle.

Unlike previous works, we focus on the potential for detecting secluded DM at the LHC, allowing the new Higgs boson to be significantly heavier. The main goal of this paper is to explore the heavy DM region in this Z_4-symmetric fermionic singlet model and to identify the viable parameter space under relic density and direct detection constraints.

*Electronic address: qxx@dlut.edu.cn
†Electronic address: haosun@dlut.edu.cn

We pay particular attention to the roles of the new scalar mass m_2 and the mixing angle $\sin\theta$, showing that a moderately small mixing is consistent with secluded DM production while still leaving room for collider searches for the additional scalar.

The paper is arranged as follows. In section II, we briefly describe the singlet fermion DM model with Z_4 symmetry. We consider the DM phenomenology and show the allowed parameter space of the model under DM relic density constraint as well as direct detection constraint in section III. In section IV, we discuss the secluded scenario of the model with the viable parameter space and determine the possible upper bound of mixing angle for the secluded DM, and we give a summary in the last section.

II. MODEL DESCRIPTION

In this part, we revisit the singlet fermionic dark matter model with Z_4 symmetry by introducing one Majorana fermion χ as a DM candidate to the SM. The bare mass term of χ is forbidden due to the Z_4 symmetry and a new singlet scalar S_0 with non-zero vacuum expectation value (vev) v_0 is also introduced so that χ will acquire mass after spontaneously symmetry breaking (SSB), and the charges the particles in the model carrying under Z_4 symmetry are listed as follows:

Particle	Z_4 charge
SM	1
S_0	-1
χ	i

TABLE I: The charges of the particles under Z_4 symmetry.

The new additional Lagrangian is therefore given as follows:

$$\mathcal{L}_{new} \supset -\frac{1}{2}\mu_0^2 S_0^2 + \frac{1}{4}\lambda_0 S_0^4 - \mu_H^2|H|^2 + \lambda_H|H|^4 + \lambda_{sh}S_0^2|H|^2 + y_{sf}S_0\chi^T\chi \tag{1}$$

where H is the SM Higgs doublet. Under unitarity gauge, H and S_0 can be expressed with:

$$H = \begin{pmatrix} 0 \\ \frac{v+h}{\sqrt{2}} \end{pmatrix}, \quad S_0 = s_0 + v_0\,, \tag{2}$$

where $v = 246$ GeV corresponds to the electroweak symmetry breaking vev and v_0 is the vev of S_0. After SSB, the mass term of χ can be given by:

$$m_\chi = y_{sf}v_0, \tag{3}$$

On the other hand, we have the squared mass matrix of s_0 and h with:

$$\mathcal{M} = \begin{pmatrix} 2\lambda_0 v_0^2 & \lambda_{sh}vv_0 \\ \lambda_{sh}vv_0 & 2\lambda_H v^2 \end{pmatrix}. \tag{4}$$

The physical masses of the two Higgs states h_1, h_2 are then

$$\begin{aligned} m_1^2 &= \lambda_H v^2 + \lambda_0 v_0^2 - \sqrt{(\lambda_H v^2 - \lambda_0 v_0^2)^2 + (\lambda_{sh}vv_0)^2}, \\ m_2^2 &= \lambda_H v^2 + \lambda_0 v_0^2 + \sqrt{(\lambda_H v^2 - \lambda_0 v_0^2)^2 + (\lambda_{sh}vv_0)^2} \end{aligned} \tag{5}$$

The mass eigenstate (h_1, h_2) and the gauge eigenstate (h, s_0) can be related via

$$\begin{pmatrix} h_1 \\ h_2 \end{pmatrix} = \begin{pmatrix} \cos\theta & -\sin\theta \\ \sin\theta & \cos\theta \end{pmatrix} \begin{pmatrix} h \\ s_0 \end{pmatrix}. \tag{6}$$

where

$$\tan 2\theta = \frac{\lambda_{sh}vv_0}{\lambda_0 v_0^2 - \lambda_H v^2} \tag{7}$$

Furthermore, we can assume h_1 is the observed SM Higgs and h_2 is the new Higgs in our model. One can choose the masses of the Higgs particles m_1 and m_2 as the inputs so that the couplings of λ_H, λ_0 and λ_{sh} can be given by:

$$\begin{aligned} \lambda_H &= \frac{(m_1^2+m_2^2)-\cos 2\theta(m_2^2-m_1^2)}{4v^2}, \\ \lambda_0 &= \frac{(m_1^2+m_2^2)+\cos 2\theta(m_2^2-m_1^2)}{4v_0^2}, \\ \lambda_{sh} &= \frac{\sin 2\theta(m_2^2-m_1^2)}{2vv_0} \end{aligned} \tag{8}$$

Note that in the case of decoupling limit with $\sin\theta \to 0$, χ relic density is completely determined by the new Higgs h_2 and we come to the so-called secluded dark matter region, where SM particles make little difference in dark matter production. On the other hand, for the non-zero $\sin\theta$ value, a pair of χs can annihilate into SM production via h_1-mediated processes, but will be suppressed for the small $\sin\theta$. Therefore, the value of $\sin\theta$ will play an important role in determining dark matter production for the secluded DM region. According to the current experiment and theoretical results, the mixing angle of the SM Higgs with other scalars is limited stringently, arising from W boson mass correction [38] at NLO, the requirement of perturbativity and unitarity of the theory [39] as well as the LHC and LEP direct search [40, 41]. The mixing in the scalar sector will suppress the couplings of h_1 to the SM quarks as well as gauge bosons by a factor of $\cos\theta$. Similarly, the couplings related to h_2 to SM quarks and gauge bosons are scaled by $\sin\theta$. A combined collier limit constraint the upper bound of $\sin\theta$ with [20]:

$$\sin\theta \lesssim \mathcal{O}(0.1) \qquad \text{for} \quad m_2 \lesssim 600\text{GeV}. \tag{9}$$

On the other hand, the mixing of the SM Higgs and the new singlet scalar will modify the electroweak precision observables such as the oblique parameters S and T. These effects will grow with the increase of the heavy Higgs and the mixing angle θ. For $m_2 \gtrsim 800$ GeV, the loop-induced corrections typically impose the bound with:

$$|\sin\theta| \lesssim 0.2. \tag{10}$$

In this work, we focus on the four free parameters with m_2,y_{sf},m_χ, as well as $\sin\theta$, and we will discuss the possible upper bound of $\sin\theta$ in the case of the secluded dark matter.

III. DARK MATTER PHENOMENOLOGY

The current observed dark matter relic density given by the Planck collaboration is $\Omega_{DM}h^2 = 0.1198 \pm 0.0012$ [42], and we consider χ as production is generated via the "Freeze-out" mechanism.

A. Boltzmann equation

The complete Boltzmann equations for the abundance of χ is given as follows:

$$\frac{dY_\chi}{dx} = -\frac{1}{3H}\frac{ds}{dx}[\langle\sigma v\rangle^{\chi\chi\to h_2h_2}(Y_\chi^2-\bar{Y}_\chi^2) + \langle\sigma v\rangle^{\chi\chi\to XX}(Y_\chi^2-\bar{Y}_\chi^2)]. \tag{11}$$

where $x = m_\chi/T$ with T being temperature, s denotes the entropy density. Y_χ is the abundance of χ defined by $Y_\chi \equiv n_\chi/s$, where n_χ is number density of χ. $\bar{Y_\chi}$ are the abundance of χ in thermal equilibrium, which is defined by:

$$\bar{Y_\chi} = \frac{45x^2}{2\pi^4 g_{*S}}K_2(x). \tag{12}$$

where $K_2(x)$ is the modified Bessel function of the second kind and g_{*S} is the number effective degrees of freedom. H is the Hubble expansion rate of the Universe, X denotes SM particles and $\langle\sigma v\rangle$ is the thermally averaged annihilation cross section. In this work, we focus on the secluded dark matter scenario, and the contribution of SM particles to χ production can be negligible compared with the annihilation of χs into h_2, which corresponds to the first term of the right-handed side of Eq. 11. We show the channels of $\chi\chi \to h_2h_2$ in Fig. 1, which include $h_1(h_2)$-mediated $s-$channel annihilation and t-channel annihilation by the exchange of χ. To calculate the DM relic density numerically, we use the micrOMGEAs 6.0 package [43]. In addition, the model has been implemented through the FeynRules package [44].

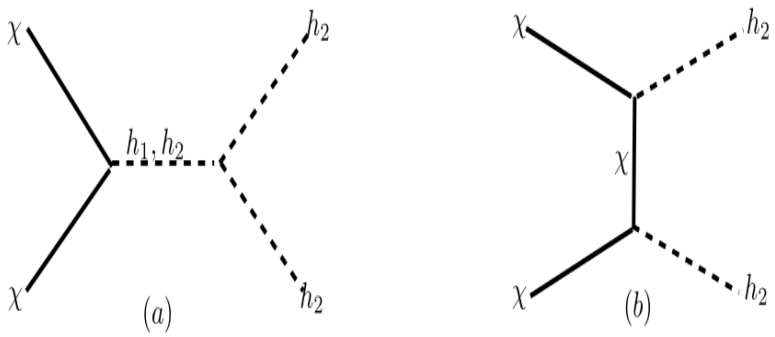

FIG. 1: Feynman diagrams of channels of $\chi\chi \to h_2 h_2$.

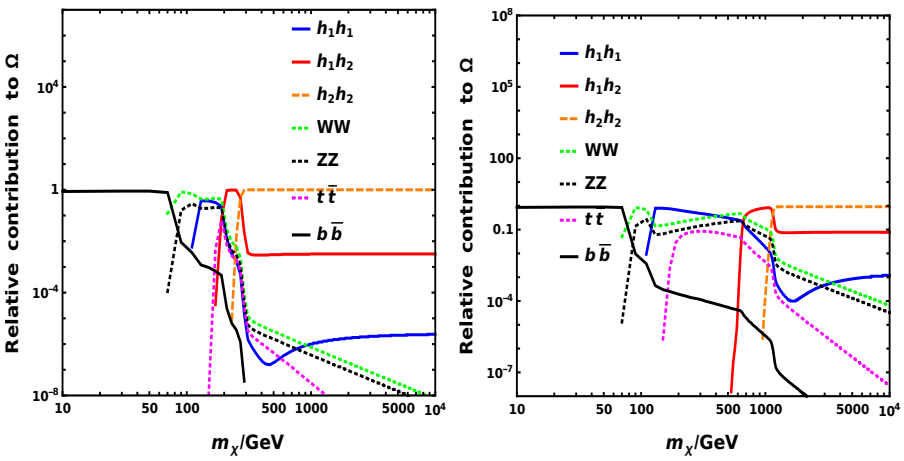

(a) (b)

FIG. 2: Relative contribution of different channels to dark matter relic density, where we set $y_{sf} = 1, m_2 = 300$ GeV and $\sin\theta = 0.003$ in the left picture and $y_{sf} = 1, m_2 = 1200$ GeV and $\sin\theta = 0.2$ in the right picture.

According to Fig. 2, we show the relative contribution of different channels to dark matter relic density with m_χ, where different colored lines represent the different annihilation production. In Fig. 2(a), we set $y_{sf} = 1$,$m_2 = 300$ GeV and $\sin\theta = 0.03$ while in Fig. 2(b) we fixed $y_{sf} = 1$,$m_2 = 1200$ GeV and $\sin\theta = 0.2$. According to Fig. 2(a), for the small m_χ with $m_\chi < m_1/2$, DM annihilation production is mainly constituted by a pair of $b\bar{b}$. Right above the SM Higgs resonance, the relative contribution of $\chi\chi \to b\bar{b}$ to DM relic density becomes smaller with the increase of m_χ, and we have other SM particles production such as $t\bar{t}$, ZZ, and $h_1 h_2$. Moreover, as $m_\chi > m_2$, it is the final state $h_2 h_2$ that almost entirely dominates the DM relic density. In Fig. 2(b), we set a larger $\sin\theta$ and heavier h_2, for $m_\chi < m_2/2$ GeV, the final states of DM annihilation are constituted by the SM particles. As $m_2/2 < m_\chi < m_2$, the relative contribution of $\chi\chi \to h_1 h_2$ increases sharply with the increase of m_2 and finally dominates over DM relic density. Similarly, when $m_\chi > m_2$, the final state $h_2 h_2$ plays a dominant role in determining DM relic density. Compared with the former case (shown in Fig. 2(a)), the relative contribution of $h_1 h_2$ is larger for the larger $\sin\theta$, and for the secluded DM region, one should have a small $\sin\theta$ to suppress the contribution of SM particles production as well as $h_1 h_2$.

B. Dependence on the parameters

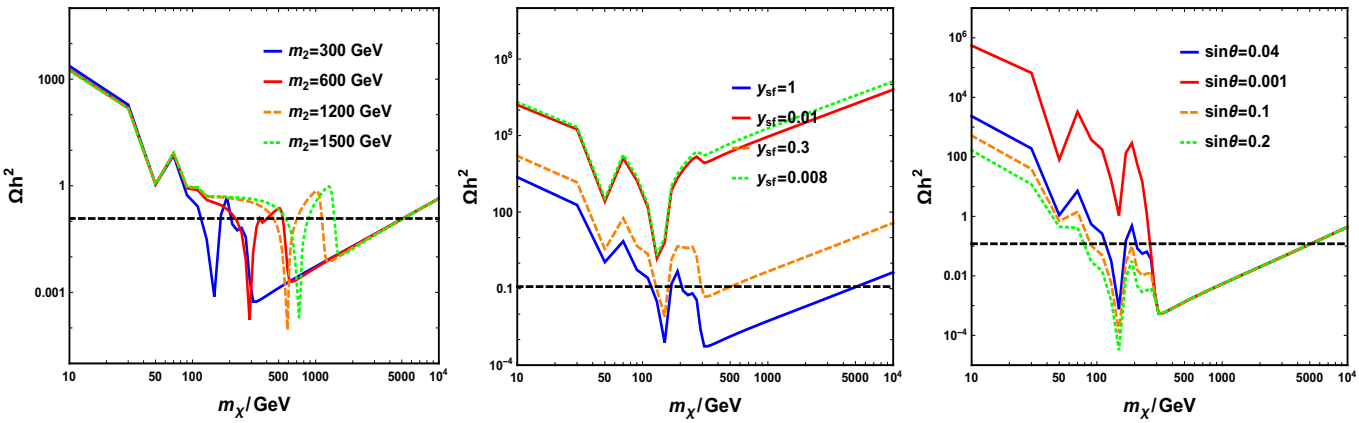

(a) (b) (c)

FIG. 3: Evolution of dark matter relic density Ωh^2 with m_χ, where the black dashed lines represent the observed value, and the blue lines are the results with $m_2 = 300$ GeV, $\sin\theta = 0.04$ as well as $y_{sf} = 1$ in the figures. Other colored lines in each pictures correspond to the results that we varied one of the parameters with other parameters unchanged.

We have four free parameters related to dark matter relic density, and in this part, we discuss the dependence on the parameters. In Fig. 3, we show the evolution of dark matter relic density Ωh^2 with m_χ, where the black dashed lines represent the observed values, and we fix $m_2 = 300$ GeV, $\sin\theta = 0.04$, as well as $y_{sf} = 1$ corresponding to the blue lines as a benchmark value. In Fig. 3(a), we vary m_2 and keep other parameters unchanged, and other different colored lines represent $m_2 = 600$ GeV, $m_2 = 1200$ GeV, and $m_2 = 1500$ GeV, respectively. As $m_\chi < m_1$, the colored lines almost coincide with each other, where χ production is entirely determined by the h_1-mediated processes related to SM particles, and h_2 makes little difference in the DM relic density. With the increase of m_χ, the line will drop sharply at $m_\chi \approx m_2/2$, where the annihilation cross section increases due to the resonance-enhanced effect. Moreover, one can also find a peak at near $m_\chi \approx m_2$, where the χ-mediated t-channel is opened, and cross section for this process goes like y_{sf}^4 and since $m_\chi \propto y_{sf}$, that process is excepted to dominant at large dark matter masses. For $m_\chi > m_2$, DM relic density is mainly determined by the t-channel process of $\chi\chi \to h_2 h_2$, and the colored lines almost coincide with each other.

According to Fig. 3(b), we vary y_{sf} and keep other parameters unchanged, and other colored lines correspond to $y_{sf} = 0.01$,$y_{sf} = 0.3$, and $y_{sf} = 0.008$ respectively. For the heavy DM mass, a larger y_{sf} can always induce a larger cross section for the t-channel process of $\chi\chi \to h_2 h_2$. On the other hand, as m_χ is small, the cross section of $\chi\chi \to XX$ is proportional to y_{sf}^2, which also means that we have a larger annihilation cross section for a larger y_{sf}. Therefore, the lines corresponding to large y_{sf} always lie below the small ones for the whole DM mass region. Moreover, for $y_{sf} = 0.01$ and $y_{sf} = 0.008$, the two lines almost coincide with each other for the small DM mass since h_1-mediated processes are dominant for the small y_{sf}.

In Fig. 3(c), we show the results by varying $\sin\theta$ and keeping other parameters unchanged, where the colored lines represent $\sin\theta = 0.001$, $\sin\theta = 0.1$, and $\sin\theta = 0.2$ respectively. As we mentioned above, for the heavy DM mass with $m_\chi > m_2$, the t-channel process of $\chi\chi \to h_2 h_2$ plays a dominant role in determining DM relic density, and the expression for the cross section is given in App. A. According to App. A, the cross section is proportional to $\cos^4\theta$, and for the small $\sin\theta$, the value of $\cos^4\theta \sim 1$, and the four colored lines almost coincide with each other for $m_\chi > 300$ GeV, as we can see in Fig. 3(c). For $m_\chi < m_2$, a larger $\sin\theta$ can always induce a larger annihilation cross section so that the lines corresponding to the small $\sin\theta$ always lie above the large ones.

As a summary, for the viable parameter space of the secluded DM scenario, one should consider that $m_\chi > m_1$ and the value of $\sin\theta$ is not too large.

C. Viable parameter space

In this model, the parameter space is constrained by the DM relic density constraint and direct detection constraint. The fermionic DM χ can interact with the nuclei through the t-channel processes of exchange of h_1 and h_2. The

effective scalar interaction can be given by [20]:

$$\mathcal{L} = \sum_q [y_{sf} \frac{m_q}{v} \sin\theta \cos\theta (\frac{1}{m_2^2} - \frac{1}{m_1^2})](\chi\chi)(\bar{q}q), \tag{13}$$

where q represent SM quarks and m_q correspond to quark masses. The spin-independent DM-nucleon scattering cross section therefore yields that:

$$\sigma_{SI} = \frac{f_N^2 m_N^4}{\pi(m_\chi + m_N)^2} [\frac{y_{sf} \sin\theta \cos\theta}{v} (\frac{1}{m_2^2} - \frac{1}{m_1^2})]^2, \tag{14}$$

where m_N is the nucleon mass and $f_N \approx 0.30$ being the form factor. To estimate the parameter space, we make a random scan to consider the viable parameter space satisfying the dark matter relic density between 0.11 and 0.13, which amounts to about a 10% uncertainty. The parameters are varied in the following ranges:

$$m_\chi \subset [40 \text{ GeV}, 10 \text{ TeV}], m_2 \subset [200 \text{ GeV}, 2000 \text{ GeV}], y_{sf} \subset [0.001, 3.14], \sin\theta \subset [10^{-6}, 0.2]. \tag{15}$$

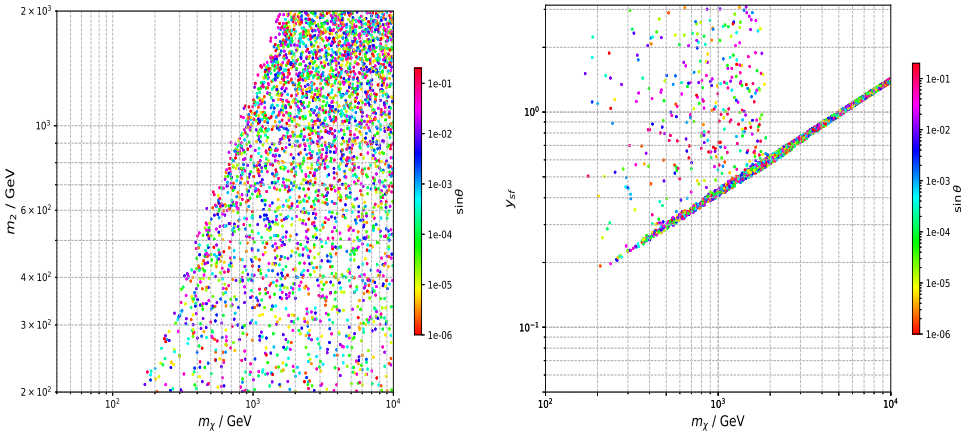

(a) (b)

FIG. 4: Viable parameter space of $m_\chi - m_2$ (left) and $m_\chi - y_{sf}$ (right) under dark matter relic density and direct detection constraints, where points with different colors correspond to the allowed value of $\sin\theta$.

In Fig. 4, we show the viable parameter space satisfying the DM relic density constraint and direct detection constraint. Points with different colors represent the allowed value of $\sin\theta$, which can take values among $[10^{-6}, 0.2]$ as we can see in Fig. 4. According to Fig. 4(a), m_2 can take value among [200 GeV, 2000 GeV], while m_χ is constrained to be larger than m_1 within the chosen parameter space. Moreover, for m_χ smaller than about 1500 GeV, most of the points lie in the lower-right region, indicating that the viable parameter space for the small m_χ is well-constrained with $m_\chi > m_2$, where $\chi\chi \to h_2 h_2$ can play a dominant role in determining DM relic density. For $m_\chi > 2$ TeV, we have $m_\chi > m_2$ and the allowed values for m_χ as well as m_2 are more flexible. In Fig. 4(b), we show the viable parameter space for $m_\chi - y_{sf}$. For $m_\chi < 2$ TeV, the allowed value for y_{sf} is flexible, and y_{sf} is constrained to be larger than about 0.19 and smaller than 3.14. As $m_\chi > 2$ TeV, m_χ is always larger than m_2 and the t-channel process of $\chi\chi \to h_2 h_2$ will be dominant as we mentioned above, and the viable value of y_{sf} is more constrained within a narrow region of $[0.2, 1.5]$ and increase with the increase of m_χ since $m_\chi \propto y_{sf}$.

IV. DISCUSSION

In this part, we discuss the secluded DM scenario of the model, we set **cut** $= \mathbf{10^{-8}}$ in the micrOMGEAs 6.0 package to pick up the relative contribution of different processes to DM relic density, where the contribution of the channel smaller than the value will be negligible during calculation, and such a tiny value can guarantee the accuracy of the results. For the secluded DM, interactions between DM and SM particles are negligible, which corresponds to the case that the contribution of $\chi\chi \to h_2 h_2$ plays a dominant role in determining DM relic density. We make a random scan following 15 but fix m_χ being a certain value.

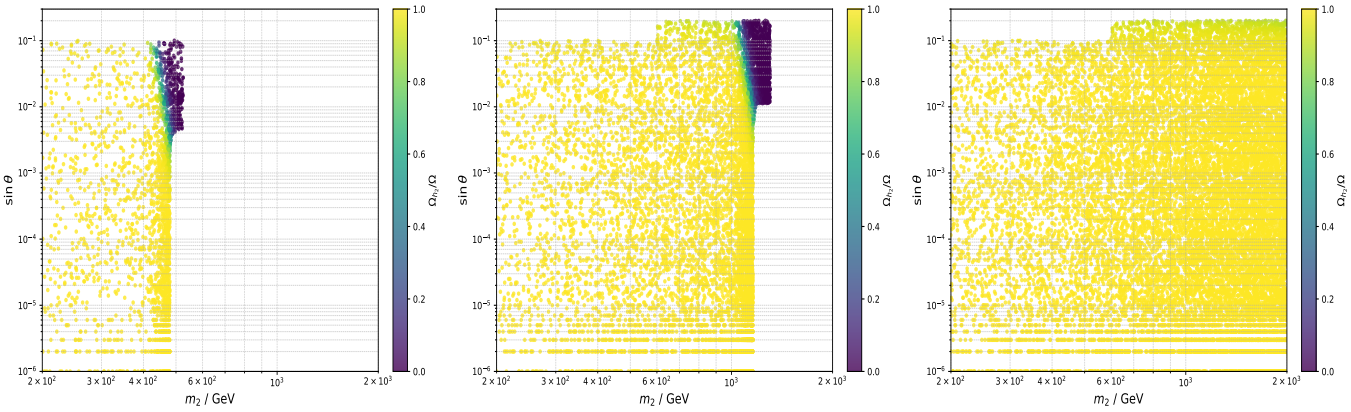

(a) (b) (c)

FIG. 5: Viable parameter space of $m_2 - \sin\theta$ with $m_\chi = 400$ GeV (a), $m_\chi = 1000$ GeV (b) and $m_\chi = 2500$ GeV (c) under dark matter relic density and direct detection constraints, where points with different colors represent contribution of $\chi\chi \to h_2 h_2$ to dark matter production defined by Ω_{h_2}/Ω.

In Fig. 5, we show the viable parameter space of $m_2 - \sin\theta$ with $m_\chi = 400$ GeV (a), $m_\chi = 1000$ GeV (b) and $m_\chi = 2500$ GeV (c) under DM relic density and direct detection constraints, where points with different colors represent contribution of $\chi\chi \to h_2 h_2$ to dark matter production defined by Ω_{h_2}/Ω. In Fig. B, we show the viable parameter space of $m_2 - y_{sf}$ respectively. According to Fig. 5(a), the allowed value for m_2 is constrained within $[200\text{ GeV}, 520\text{ GeV})$, and for $m_2 < m_\chi$, contribution of $\chi\chi \to h_2 h_2$ will play a dominant role in determining DM relic density, and $\sin\theta$ can take value among $[10^{-6}, 0.1]$. Note that here the allowed value for m_2 is smaller than 600 GeV and we have $\sin\theta < 0.1$ according to the constraint on the mixing angle. For $m_2 < 400$ GeV, the value of $\sin\theta$ is flexible and can take a value among $[10^{-6}, 0.1]$ under the DM relic density constraint and direct detection constraint. Moreover, the fraction Ω_{h_2}/Ω is approximately equal to 1, which indicates that the process $\chi\chi \to h_2 h_2$ always plays a dominant role in determining DM relic density regardless of the value of $\sin\theta$. For $m_2 > 400$ GeV and $m_\chi < m_2$, the annihilation process is suppressed, and SM particles can also contribute to DM production. When m_χ is smaller than about 500 GeV, the fraction Ω_{h_2}/Ω is determined by the allowed value of $\sin\theta$. Concretely speaking, as $\sin\theta$ is larger than 10^{-3}, the fraction Ω_{h_2}/Ω is much smaller compared with the results of $m_\chi > m_2$, and dark matter production is mainly determined by SM particles. Contrarily, if $\sin\theta$ is smaller than 10^{-3}, the fraction is approximately equal to 1, and the contribution of SM particles can be negligible, and DM production can be obtained via the "Forbidden channel" of $\chi\chi \to h_2 h_2$, where the process is forbidden at zero temperature and kinetically allowed at high temperature. For $m_2 > 500$ GeV, the allowed value for $\sin\theta$ is constrained to be larger than 4×10^{-3} and the fraction is much smaller where χ will mainly annihilate into SM particles. Therefore, for the secluded DM, we have two possible viable regions for m_2 with $m_\chi = 400$ GeV: larger than 200 GeV but smaller than m_χ and m_2 is degenerate with m_χ. For the former case, the allowed $\sin\theta$ value is flexible and can take a value among $[10^{-6}, 0.1]$, while for the latter case, $\sin\theta$ is constrained to be smaller than 10^{-3} under the DM relic density constraint. In Fig. 5(b), we fix $m_\chi = 1000$ GeV, and we have a similar conclusion for the viable parameter space of $m_2 - \sin\theta$ as well as the fraction Ω_{h_2}/Ω. Note that the allowed value for m_2 is about $[200\text{ GeV}, 1200\text{ GeV}]$, and we have $\sin\theta \leqslant 0.1$ for $m_2 < 600$ GeV and $\sin\theta \leqslant 0.2$ for $600\text{ GeV} < m_2 < 1200$ GeV according to the constraints arising from mixing angle. As $m_2 < m_\chi$ and m_2 is degenerate with m_χ for $\sin\theta < 2 \times 10^{-3}$, the fraction is approximately equal to 1, and we come to the secluded DM region. When m_2 is larger than about 1000 GeV and $\sin\theta$ is larger than 2×10^{-3}, the annihilation production of χ is almost constituted by SM particles. In Fig. 5(c), we show the result of $m_\chi = 2500$ GeV, where m_χ is always larger than m_2 within the chosen parameter space, both m_2 and $\sin\theta$ are flexible under DM relic density constraint and direct detection constraint, and the process $\chi\chi \to h_2 h_2$ always plays a dominant role in determining DM relic density. To estimate the parameter space of the secluded DM region, we constrain the fraction equal to 100% stringently to obtain the upper bound of $\sin\theta$. We show the contour plot of $m_2 - \sin\theta$ under DM relic density constraint and direct detection constraint, where the legend corresponds to the fraction and the red dashed lines represent the upper bound of $\sin\theta$ as the fraction equals 100%. In Fig. 6(a), we fix $y_{sf} = 1, m_\chi = 400$ GeV and the maximum of $\sin\theta$ is 0.003, which indicates that we have secluded DM as long as $\sin\theta < 0.003$. The allowed value for m_2 is stringently constrained with a narrow region for secluded DM. We have a similar conclusion for Fig. 6(b) with $y_{sf} = 1$ and $m_\chi = 1000$ GeV, where the upper bound of $\sin\theta$ is 0.007 and m_2 should be larger than 1050 GeV and smaller than 1100 GeV for the secluded DM. In Fig. 6(c), we set $y_{sf} = 0.66$ and $m_\chi = 2500$ GeV. Note that m_χ

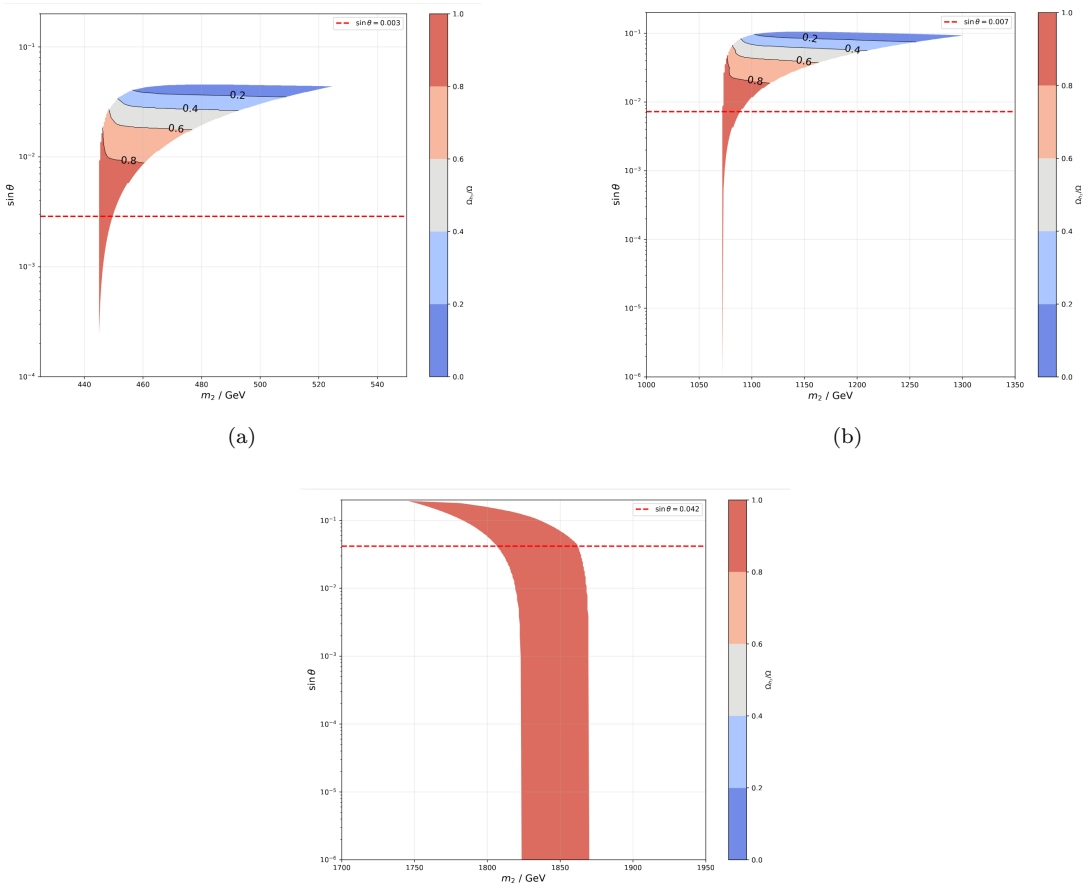

(a) (b) (c)

FIG. 6: Similar with Fig. 5 but we fix $y_{sf} = 1$,$m_\chi = 400$ GeV (a), $y_{sf} = 1$, $m_\chi = 400$ $m_\chi = 1000$ GeV (b) and $y_{sf} = 0.66, m_\chi = 2500$ GeV (c), and the red dashed lines correspond to the upper bound of $\sin\theta$ in the case of dark matter production is totally determined by the process of $\chi\chi \to h_2 h_2$.

is always larger than m_2 in this case, and the annihilation process $\chi\chi \to h_2 h_2$ is kinetically allowed within the chosen parameter space, where the fraction is approximately equal to 1. For the secluded DM, the upper bound of $\sin\theta$ is 0.042, and the allowed value for m_2 is more flexible and can take a value within about (1800 GeV, 1875 GeV). As a summary, for the secluded DM, m_χ should be larger than m_2 or m_2 and m_χ are degenerate under DM relic density constraint, and a larger m_χ always demands a larger m_2 to obtain the observed result. Moreover, for the larger m_χ, the upper bound of $\sin\theta$ is larger, as we can see in Fig. 6.

On the other hand, the non-zero $\sin\theta$ gives the possibility to search for secluded DM of the model in future collider experiments for the secluded DM even though the interactions between DM and SM particles are suppressed. Particularly, as we mentioned above, when m_χ is large, the upper bound of $\sin\theta$ can be at $\mathcal{O}(0.04)$ level. The new Higgs h_2 will couple to SM fermions as well as gauge bosons through mixing with the SM Higgs boson, and can therefore be produced in large quantities at the LHC via mechanisms such as gluon-gluon fusion(ggF) and vector boson fusion (VBF), with the cross sections proportional to $\sin^2\theta$. Furthermore, for the decay of h_2 to $\chi\chi$, the decay width may be much larger than that of h_2 decaying into SM particles. Consequently, its resonance production, accompanied by a signal with a large missing transverse energy (MET), becomes a golden channel for searching for DM. The allowed value of m_2 can range from several hundred GeV to the TeV scale, covering the mass range extensively explored by the LHC and future colliders.

When $\sin\theta$ is small and y_{sf} is large for the secluded DM scenario, h_2 decays invisibly, and its production results in DM final states. In this case, the resonant process $pp \to h_2 \to \chi\chi$ can be probed at the LHC, where h_2 is produced resonantly and subsequently decays into a pair of DM particles. This process yields a signature with large missing transverse energy (MET), representing the most typical probe and providing the largest possible cross-section for this model in collider experiments. However, for the invisible decay of h_2, the signal consists solely of MET, requiring

initial-state radiation (ISR) to furnish an observable trigger. One viable channel is $pp \to h_2(\to \chi\chi) + Z$, where the Z gauge boson subsequently decays into a pair of leptons or invisible neutrinos. The advantage of this process lies in its clean background, with possible backgrounds including ZZ, WZ, and $t\bar{t}Z$.

If $\sin\theta$ is large and y_{sf} is small for the secluded DM as we mentioned above, the new Higgs boson h_2 can act as a scalar resonance state directly observable via the visible mode. Such signals have the advantage of strong background suppression due to the narrow-width resonance peak of h_2. One possible process related to DM production at the LHC is $pp \to h_2(h_2 \to ZZ) + \chi\chi$, and χ arises from the h_2 invisible decay branch, and we have subsequent decay of h_2 with $h_2 \to ZZ \to 4l$, where l represents leptons. The clean background facilitates signal reconstruction, and the MET primarily originates from the accompanying dark matter.

V. SUMMARY AND OUTLOOK

The WIMP paradigm faces a serious challenge from the null results of DM direct detection experiments, which impose the most stringent constraints on DM parameter space. One possible solution to alleviate this tension is secluded DM, where the interactions between DM and SM particles can be negligible, thereby evading direct detection constraints. In this work, we revisit the singlet fermionic dark matter model, assuming a Majorana fermion χ carrying a Z_4 charge as the DM candidate. The Z_4 symmetry forbids a bare mass term for χ, and a new singlet scalar with a non-zero vacuum expectation value (vev) is introduced. As a result, χ acquires mass, and after spontaneous symmetry breaking (SSB), two Higgs bosons emerge, with the lighter one identified as the SM Higgs boson.

We focus on the secluded DM region of the model, where the mixing angle between the two Higgs bosons plays a crucial role in determining the DM production, depending on the mass hierarchy between the new Higgs mass and the DM mass. In this secluded region, the dominant annihilation channel of χ is into a pair of new Higgs bosons, $\chi\chi \to h_2 h_2$, while its interactions with SM particles are highly suppressed. This suppression allows the model to naturally evade the stringent constraints from direct detection experiments, which have severely limited the traditional WIMP parameter space.

We have systematically analyzed the dependence of the DM relic density on the four free parameters of the model: the new Higgs mass m_2, the Yukawa coupling y_{sf}, the DM mass m_χ, and the mixing angle $\sin\theta$. Our numerical results reveal that the relic density is dominated by the t-channel process $\chi\chi \to h_2 h_2$, whose cross section is proportional to $\cos^4\theta$, making it largely insensitive to $\sin\theta$ in the small-mixing limit. Conversely, when $m_\chi \sim m_2/2$ or $m_\chi \sim m_2$, resonance effects can significantly enhance the annihilation cross section. We perform a random scan of the model's parameter space to estimate the allowed regions. Our scan results indicate that a viable secluded DM scenario exists over a wide range of masses. Furthermore, we discuss the upper bound on $\sin\theta$ for a fixed DM mass in the secluded region, finding that the upper bound increases with m_χ. These results imply that the secluded DM region is not confined to extremely small mixing angles; rather, moderately small values of $\sin\theta \sim \mathcal{O}(0.01 - 0.04)$ are allowed for TeV-scale DM. We note that a certain cut value has been adopted in our analysis to define the secluded scenario, ensuring that the contribution from SM particles to DM production is negligible. While a tighter cut would yield more accurate results, the overall conclusion regarding the mixing angle remains unchanged. The non-zero mixing angle opens up promising search channels for the secluded DM region. In particular, the new scalar h_2 can be produced at colliders, offering complementary probes at current and future facilities, including the High-Luminosity LHC and proposed e^+e^- colliders.

Appendix A: Formulas

In this part, we give the expression of the cross section for t-channel process of $\chi\chi \to h_2 h_2$ shown in Fig. 1(b):

$$\begin{aligned}\sigma =& \frac{2\cos^4\theta y_{sf}^4}{\pi s(s-4m_\chi^2)}\Big(\frac{(-4m_2^2(4m_\chi^2+s)+6m_2^4+16m_\chi^2 s-32m_\chi^4+s^2)\log\big(\frac{-\sqrt{(s-4m_2^2)(s-4m_\chi^2)}-2m_2^2+s}{\sqrt{(s-4m_2^2)(s-4m_\chi^2)}-2m_2^2+s}\big)}{2m_2^2-s} \\ &-\frac{\sqrt{(s-4m_2^2)(s-4m_\chi^2)}(-16m_2^2m_\chi^2+3m_2^4+2m_\chi^2(8m_\chi^2+s))}{-4m_2^2m_\chi^2+m_2^4+m_\chi^2 s}\Big)\end{aligned} \tag{A1}$$

where s is the squared center-of-mass energy. According to Eq. A1, the cross section is proportional to $\cos^4\theta$, and this value is approximately equal to 1, which makes little difference in DM relic density for the small $\sin\theta$.

Appendix B: Viable parameter space for $m_2 - y_{sf}$

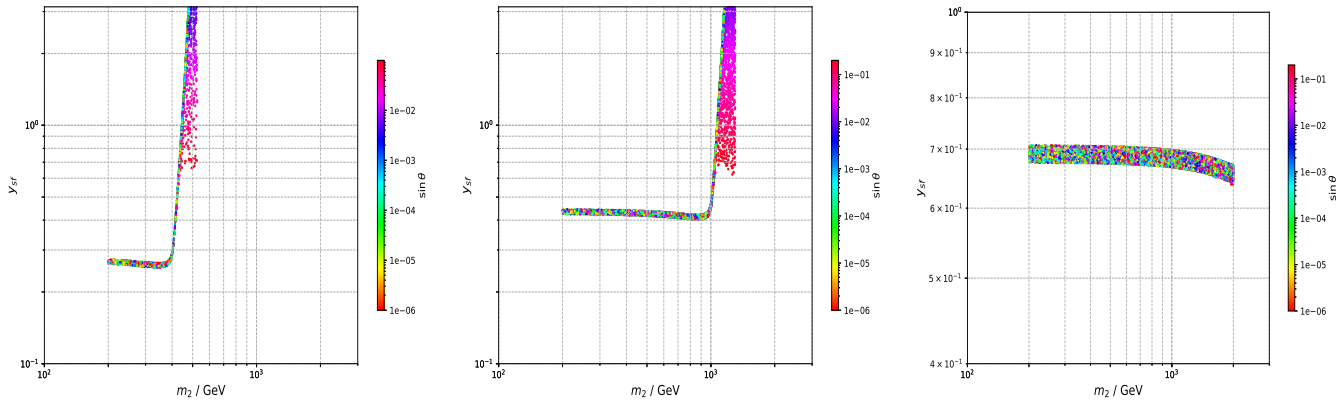

(a) (b) (c)

FIG. 7: Viable parameter space of $m_2 - y_{sf}$ with $m_\chi = 400$ GeV (a), $m_\chi = 1000$ GeV (b) and $m_\chi = 2500$ GeV (c) under dark matter relic density and direct detection constraints, where points with different colors represent the allowed value for $\sin\theta$.

In this part, we show the scan results of Fig. 5 for $m_2 - y_{sf}$ with $m_\chi = 400$ GeV (a), $m_\chi = 1000$ GeV (b) and $m_\chi = 2500$ GeV (c) under dark matter relic density and direct detection constraints, where points with different colors represent the allowed value for $\sin\theta$ and can take value among $[10^{-6}, 0.2]$. According to Fig. 7(a), the allowed value for m_2 is about $[200\text{ GeV}, 520\text{ GeV}]$ and y_{sf} is constrained to be larger than 0.25 for $m_\chi = 400$ GeV. As $200\text{ GeV} \leqslant m_2 \leqslant 400\text{ GeV}$, y_{sf} is constrained within a narrow region, where DM production is mainly determined by a pair of h_2 annihilation. For $m_2 > m_\chi$, SM particles can also contribute to DM relic density, and the allowed value for y_{sf} is more flexible and can take a value among $(0.25, 3.14]$. Particularly, when $m_2 > 500$ GeV, a large y_{sf} always demands a small $\sin\theta$ to obtain the correct DM relic density, as we can see in Fig. 7(a). We have similar results for $m_\chi = 1000$ GeV according to Fig. 7(b), where the allowed value for y_{sf} is divided into two regions depending on the relationship between m_χ and m_2. In Fig. 7(c), the value of m_2 is always smaller than m_χ with $m_\chi = 2500$ GeV, and y_{sf} is constrained within a narrow region with $0.6 < y_{sf} < 0.72$ while we have $200\text{ GeV} \leqslant m_2 \leqslant 2000\text{ GeV}$, where DM relic density is determined by the process $\chi\chi \to h_2 h_2$. Moreover, when $m_2 > m_\chi/2$, the upper bound as well as the lower bound of y_{sf} are smaller with the increase of m_2 under the DM relic density constraint.

Acknowledgments

Hao Sun is supported by the National Natural Science Foundation of China (Grant No.12075043, No.12147205).XinXin Qi is supported by the National Natural Science Foundation of China (Grant No.12447162).

[1] Y. Meng et al. (PandaX-4T), Phys. Rev. Lett. **127**, 261802 (2021), 2107.13438.
[2] J. Aalbers et al. (LZ) (2024), 2410.17036.
[3] M. Pospelov, A. Ritz, and M. B. Voloshin, Phys. Lett. B **662**, 53 (2008), 0711.4866.
[4] K.-C. Yang, JHEP **07**, 148 (2020), 2001.04946.
[5] C. Siqueira, Phys. Lett. B **797**, 134840 (2019), 1901.11055.
[6] G. N. Fortes, F. S. Queiroz, C. Siqueira, and A. Viana, JCAP **07**, 043 (2023), 2212.05075.
[7] M. Pospelov and A. Ritz, Phys. Lett. B **671**, 391 (2009), 0810.1502.
[8] A. Dedes, I. Giomataris, K. Suxho, and J. D. Vergados, Nucl. Phys. B **826**, 148 (2010), 0907.0758.
[9] B. Batell, M. Pospelov, A. Ritz, and Y. Shang, Phys. Rev. D **81**, 075004 (2010), 0910.1567.
[10] B. von Harling and K. L. McDonald, JHEP **08**, 048 (2012), 1203.6646.
[11] E. C. F. S. Fortes, V. Pleitez, and F. W. Stecker, Astropart. Phys. **74**, 87 (2016), 1503.08220.
[12] S. Adrián-Martínez et al. (ANTARES), JCAP **05**, 016 (2016), 1602.07000.
[13] S. Okawa, M. Tanabashi, and M. Yamanaka, Phys. Rev. D **95**, 023006 (2017), 1607.08520.
[14] M. Ardid, I. Felis, A. Herrero, and J. A. Martínez-Mora, JCAP **04**, 010 (2017), 1701.08863.

[15] C. Siqueira, G. N. Fortes, A. Viana, and F. S. Queiroz, PoS **ICRC2021**, 577 (2021), 2107.04053.
[16] P. Bandyopadhyay, M. Mitra, R. Padhan, A. Roy, and M. Spannowsky, JHEP **05**, 182 (2022), 2201.09203.
[17] A. Albert et al. (ANTARES), JCAP **06**, 028 (2022), 2203.06029.
[18] P. S. B. Dev, J. Gehrlein, A. Sengupta, and A. Soni (2026), 2605.28923.
[19] E. Ma, P. K. Paul, and N. Sahu, Phys. Rev. D **112**, 095020 (2025), 2508.02642.
[20] J. Das, S. Niyogi, and T. Srivastava, JCAP **06**, 018 (2026), 2601.13147.
[21] C. E. Yaguna and Ó. Zapata, JCAP **06**, 049 (2024), 2401.13101.
[22] B. Díaz Sáez, P. Escalona, S. Norero, and A. R. Zerwekh, JHEP **10**, 233 (2021), 2105.04255.
[23] Y. G. Kim, K. Y. Lee, and S. Shin, JHEP **05**, 100 (2008), 0803.2932.
[24] Y. G. Kim, K. Y. Lee, and S.-h. Nam (2025), 2506.20113.
[25] C. E. Yaguna and Ó. Zapata, Phys. Rev. D **109**, 015002 (2024), 2308.05249.
[26] D.-W. Jung, S.-H. Nam, C. Yu, Y. G. Kim, and K. Y. Lee, Eur. Phys. J. C **80**, 513 (2020), 2002.10075.
[27] Y. G. Kim, C. B. Park, and S. Shin, JHEP **12**, 036 (2018), 1809.01143.
[28] J. Hisano, R. Nagai, and N. Nagata, JHEP **12**, 059 (2018), 1808.06301.
[29] S. Bhattacharya, I. de Medeiros Varzielas, B. Karmakar, S. F. King, and A. Sil, JHEP **12**, 007 (2018), 1806.00490.
[30] Y. G. Kim, K. Y. Lee, and S.-H. Nam, Phys. Lett. B **782**, 316 (2018), 1801.04074.
[31] M. Ettefaghi and R. Moazzemi, Eur. Phys. J. C **77**, 343 (2017), 1705.07571.
[32] J. Sheng and T. T. Yanagida, Phys. Rev. D **113**, 055010 (2026), 2510.17370.
[33] Y. Georis, J. Sheng, S. Urrea, and T. T. Yanagida, JHEP **04**, 004 (2026), 2512.13158.
[34] Z. Wang, Y. Reyimuaji, and N. Yalikun, Phys. Rev. D **112**, 055041 (2025), 2412.15672.
[35] J. Guo, Z. Kang, and P. Zhang, Phys. Lett. B **826**, 136885 (2022), 2108.12964.
[36] Y. G. Kim, K. Y. Lee, C. B. Park, and S. Shin, Phys. Rev. D **93**, 075023 (2016), 1601.05089.
[37] S. Profumo, F. S. Queiroz, J. Silk, and C. Siqueira, JCAP **03**, 010 (2018), 1711.03133.
[38] D. López-Val and T. Robens, Phys. Rev. D **90**, 114018 (2014), 1406.1043.
[39] T. Robens, in 55th Rencontres de Moriond on QCD and High Energy Interactions (2021), 2105.07719.
[40] V. Khachatryan et al. (CMS), JHEP **10**, 144 (2015), 1504.00936.
[41] M. J. Strassler and K. M. Zurek, Phys. Lett. B **661**, 263 (2008), hep-ph/0605193.
[42] N. Aghanim et al. (Planck), Astron. Astrophys. **641**, A6 (2020), 1807.06209.
[43] G. Alguero, G. Belanger, F. Boudjema, S. Chakraborti, A. Goudelis, S. Kraml, A. Mjallal, and A. Pukhov, Comput. Phys. Commun. **299**, 109133 (2024), 2312.14894.
[44] A. Alloul, N. D. Christensen, C. Degrande, C. Duhr, and B. Fuks, Comput. Phys. Commun. **185**, 2250 (2014), 1310.1921.